Acoustic streaming induced by ultrasonic flexural vibrations and associated enhancement of convective heat transfer

Byoung-Gook Loh
Precision Engineering Center, North Carolina State University, Raleigh, North Carolina 27695-7910

Sinjae Hyun
Mechanical and Aerospace Engineering Department, North Carolina State University, Raleigh, North Carolina 27695-7910

Paul I. Ro
Precision Engineering Center, North Carolina State University, Raleigh, North Carolina 27695-7910

Clement Kleinstreuer
Mechanical and Aerospace Engineering Department, North Carolina State University, Raleigh, North Carolina 27695-7910

(Received 29 January 2001; accepted for publication 31 October 2001)

Acoustic streaming induced by ultrasonic flexural vibrations and the associated convection enhancement are investigated. Acoustic streaming pattern, streaming velocity, and associated heat transfer characteristics are experimentally observed. Moreover, analytical analysis based on Nyborg's formulation is performed along with computational fluid dynamics (CFD) simulation using a numerical solver CFX 4.3. Two distinctive acoustic streaming patterns in half-wavelength of the flexural vibrations are observed, which agree well with the theory. However, acoustic streaming velocities obtained from CFD simulation, based on the incompressible flow assumption, exceed the theoretically estimated velocity by a factor ranging from 10 to 100, depending upon the location along the beam. Both CFD simulation and analytical analysis reveal that the acoustic streaming velocity is proportional to the square of the vibration amplitude and the wavelength of the vibrating beam that decreases with the excitation frequency. It is observed that the streaming velocity decreases with the excitation frequency. Also, with an open-ended channel, a substantial increase in streaming velocity is observed from CFD simulations. Using acoustic streaming, a temperature drop of 40 °C with a vibration amplitude of 25 μm at 28.4 kHz is experimentally achieved. [DOI: 10.1121/1.1433811]

PACS numbers: 43.40.At [PJR]

I. INTRODUCTION

Acoustic streaming is a steady circular airflow occurring in a high-intensity sound field. Two factors have been known to induce acoustic streaming: spatial attenuation of a wave in a free space and the friction between a medium and a vibrating object (cf. Lee and Wang, 1990). When sound waves propagate, they are attenuated by absorption and scattered. This attenuation is, in general, insignificant in a short distance of propagation. However, the propagation of a high-intensity sound wave results in the attenuation of pressure significant enough to create steady bulk airflow. This type of streaming is usually associated with a medium of high viscosity. The other type of acoustic streaming is attributed to the friction between a vibrating medium in contact with a solid wall (cf. Ingard and Labate, 1950; Nyborg, 1958). As long as there is an oscillating tangential relative velocity, it is not important whether the source of a relative motion arises from either acoustic oscillations in the fluid or vibrations of the solid. Both cases lead to frictional dissipation within Stokes boundary layer. Unlike acoustic streaming resulting from spatial attenuation, this streaming has two components: inner and outer streaming. The inner streaming is created within the boundary layer due to the friction between the medium and the wall. Then, the inner streaming, in turn, induces relatively large-scale steady streaming outside the boundary layer. This process can be compared to the generation of electromagnetic field by a surface current on a conductor (cf. Lee and Wang, 1990). It is reported that the acoustic streaming is especially effective in promoting certain kinds of rate process occurring on the solid and fluid interface including convective heat transfer, electrical effects, changes in biological cells, and removal of loosely adhering surface layers (cf. Nyborg, 1958).

Faraday (1831) found that currents of air rise at displacement anti-nodes on plates and descend at the nodes. Rayleigh (1945) performed the first theoretical analysis of the acoustic streaming phenomenon. Further developments of the theory were made by Schlichting (1955), Nyborg (1958), and Lighthill (1978), where emphasis was placed on the fundamental role of dissipation of the acoustic energy in the evolution of the gradients in the momentum flux. In the study of Jackson and Nyborg (1960), acoustic streaming induced by sonic longitudinal vibration is investigated. Acoustic streaming induced by ultrasonic flexural traveling waves is studied for a micropump application and negligible heat transfer capability of acoustic streaming is reported (cf. Nguyen and White, 1999). Fand and Kave (1960) and Gould

(1966) studied heat transfer across a solid–liquid interface in the presence of sonically induced acoustic streaming and found that the effect of acoustic streaming was to cause the convective heat transfer rate from the heated cylinder to increase by a factor of 3. Gopinath and Mills (1993, 1994) investigated convective heat transfer due to acoustic streaming across the ends of a Kundt tube. Selected references give an overview of the works done for investigating the heat transfer characteristics of acoustic streaming (cf. Uhlenwinkel *et al.*, 1994; Vainshtein *et al.*, 1995; Chen *et al.*, 1998).

Most previous studies concentrated on acoustic streaming induced by sonic longitudinal vibration in an enclosed space such as a Kundt tube. Not much research on acoustic streaming induced in an open space by ultrasonic flexural vibration has been carried out. Ultrasonic excitation significantly increases acoustic streaming velocity. As a result, corresponding convective heat transfer rate can grow to the extent equal to that of conventional fan-based cooling. In addition, ultrasonic excitation permits silent operation. Employing flexural vibrations as a source of acoustic streaming allows for a slim profile and low power operation because flexural impedance of an elastic beam is generally far smaller than longitudinal impedance. To take full advantage of this promising technology, it is imperative to understand the nature of formation of acoustic streaming, its transient characteristics, streaming velocity, and associated enhancement of convective heat transfer.

Therefore, the objective of this article is to investigate the momentum and heat transfer due to the acoustic streaming induced by ultrasonic flexural vibrations in an open environment. A primary focus is placed on experimental observations of the phenomenon, simulations employing computational fluid dynamics software (CFX4), comparison with the existing analytical solution by Nyborg (1958), and cooling property.

II. EXPERIMENTAL OBSERVATIONS

A. Experimental apparatus

The experimental setup shown in Fig. 1 consists of a beam and modules that contain a piezoelectric actuator and a horn. The beam and horn are made of 6061-T6 aluminum due to its excellent acoustical characteristics. The piezoelectric actuator is a bolted Langevin type transducer (BLT) designed to resonate at 28 kHz (Sashida, 1993). The conical horn is used to increase the amplitude of vibration provided by the actuator. A conical geometry was chosen because it not only gives a desired amplification ratio but also can be easily machined. A mounting flange was included in the design of the horn and is located at the nodal lines where the velocity of vibration of the horn goes to zero. This allowed the mounting of the horn and BLT assembly onto a supporting base plate that was in turn bolted to the surface of an air-driven vibration absorption table. The small end of the horn was threaded to connect the beam with the horn using a machine screw. The dimension of the beam is determined such that one of the natural frequencies of the beam is located in the vicinity of the resonant frequency of the actuator,

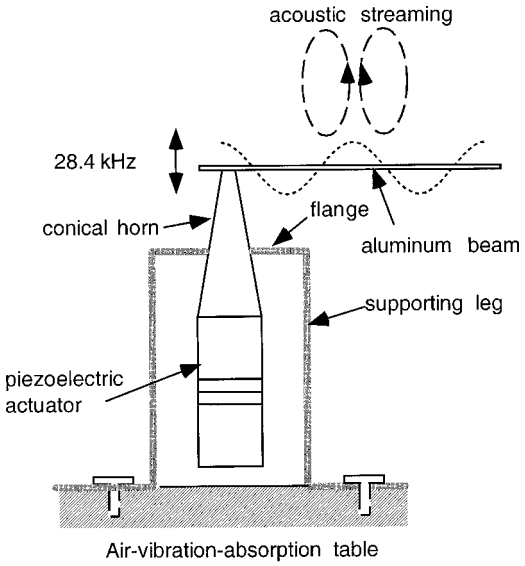

FIG. 1. Experimental setup.

thereby maximizing the displacement of the beam for a given power supply. The determined dimension is 10 mm wide, 1 mm thick, and 128 mm long. Frequency spectrum analysis of the system reveals that at an excitation frequency of 28.4 kHz, maximum vibration amplitude of the beam is achieved.

B. Acoustic streaming near the vibrating beam

To visualize acoustic streaming near the beam, the beam is excited at 28.4 kHz with the vibration amplitude of 10 μm. Acetone is sprayed onto the vibrating beam. When acetone comes in contact with the beam, it becomes small droplets and follows the airflow pattern near the beam until it completely evaporates. A fiber optic lamp locally illuminates the region near the vibrating beam. Light is reflected from only acetone droplets and the beam, making ambient air appear black. The whole process is videotaped using a camcorder. Figure 2 shows a snap shot of the process. Unique features of acoustic streaming are observed. First, air rises above the antinodes and descends toward the nodes. Since vibration amplitude is not uniform along the length of the beam, the maximum distance to which acetone droplets rise above the antinodes are not uniform either. Second, there exist two

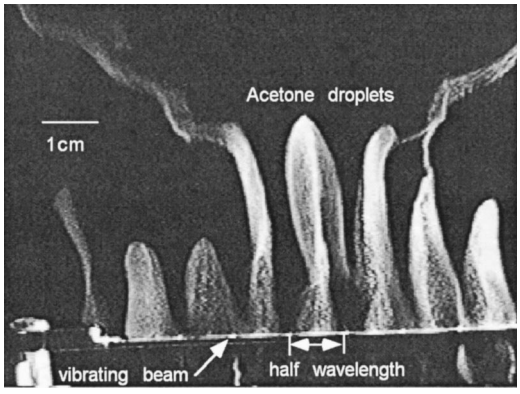

FIG. 2. Acoustic streaming over a ultrasonically vibrating beam.

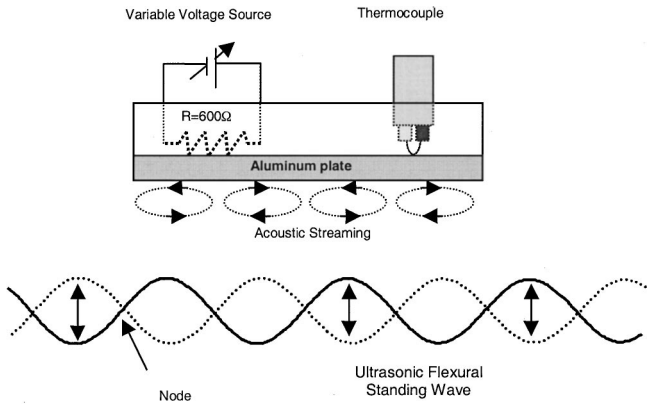

FIG. 3. Experimental setup for measuring enhancement of heat transfer.

distinctive circular airflows within the half-wavelength of the beam (1 cm for this case). Clearer acoustic streaming is observed with bigger vibration amplitude.

C. Streaming in the gap

One interesting application of acoustic streaming considered in this study is the enhancement of convective heat transfer. To this end, it is possible to envision that a heated object is placed over a vibrating beam near which acoustic streaming is induced. Then, the temperature of the heated object is decreased due to forced convection caused by acoustic streaming. Therefore, for heat transfer application, it is important to study how the acoustic streaming pattern changes when there is a stationary upper beam that represents a heat source.

A beam that is 1 cm wide, 2.5 cm thick, and 11 cm long is placed 1 cm over the vibrating beam. The same visualization process used for the case without an upper stationary beam is performed at the gaps ranging from 2 mm to 1 cm. It is observed that acoustic streaming in the gap is strong enough to blow most acetone droplets out of the gap, making it almost impossible to perform visual observation of acoustic streaming pattern. Therefore, CFD simulation presented in Sec. IV is used to estimate acoustic streaming pattern and velocity in the gap.

D. Enhancement of convective heat transfer

To measure the enhancement of convective heat transfer due to acoustic streaming, a heat source containing an aluminum plate, a resistor, and a thermocouple is made. A detailed schematic drawing of the plate is shown in Fig. 3. The bottom of the plate is made of aluminum. The top is made of Plexiglas that contains a 600-Ω resistor and a thermocouple. The resistor is connected to a variable voltage power supply and serves as a heater.

With the 600 Ω resistor, the temperature of the plate can be increased to 98 °C with the available power supply of 3.4 W. During the experiment, the room temperature was kept at 20 °C. The heat source is placed 1.5 mm above the vibrating beam. As the temperature of the heat source reaches a steady-state value of 98 °C, acoustic streaming is generated by vibrating the beam at 28.4 kHz with the vibration amplitude of 10 μm. Then, the temperature changes of the plate

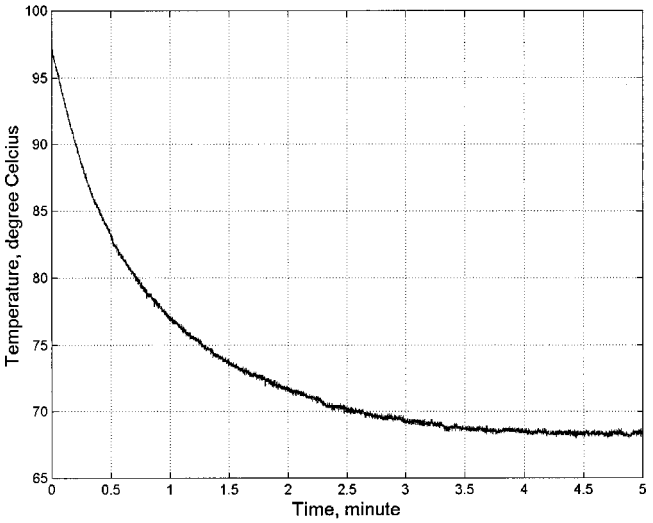

FIG. 4. Measurement of temperature drop of the heat source.

are measured using a thermocouple. Due to the inherent noises in the voltage signal from the thermocouple, the signal is filtered through a low-pass filter and sampled at 20 Hz using a data acquisition board. A temperature drop of 30 °C is achieved in 4 min and maintained as shown in Fig. 4. As the vibration amplitude is further increased to 25 μm, a temperature drop of 40 °C is achieved that is the maximum temperature drop obtained with the current experimental setup.

When acoustic streaming is induced in the gap, there are two possible major heat flow paths. The first one is convective heat transfer to ambient air in the direction parallel to the heat source marked as heat flow path 1 in Fig. 5. In this path, the heat from the heat source is taken away by airflow near the heat source and transferred to ambient air at both sides of the gap. The second path is convective heat transfer through the vibrating beam marked as heat flow path 2. Due to the recirculating nature of acoustic streaming flow pattern, in the second path the heat from the heat source is transferred to the vibrating beam and dissipated to ambient air.

To measure the heat transfer in path 1, the space between the heat source and the vibrating beam is enclosed along the perimeter of heat source, thereby allowing heat to flow only in path 2. As shown in Fig. 6, for the enclosed gap case, the achieved temperature drop is 10 °C less than for the open gap system, which is about a 33% decrease in the tem-

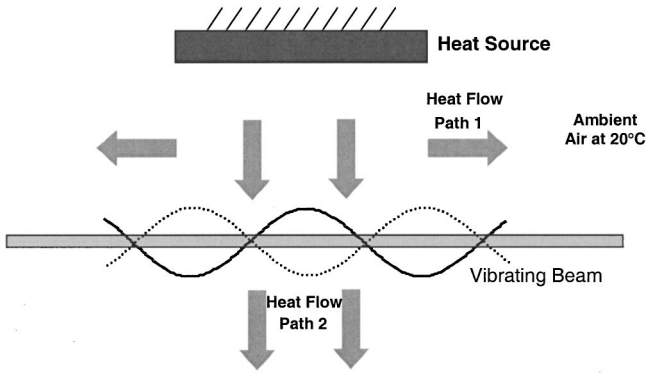

FIG. 5. Heat flow paths.

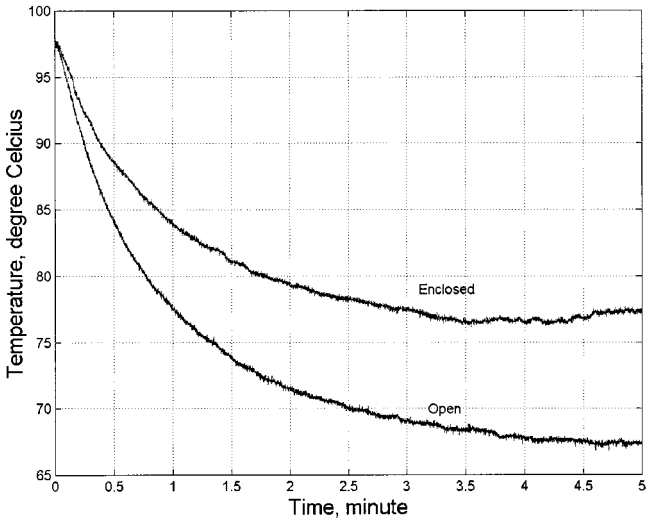

FIG. 6. Effect of enclosing the heat source.

perature drop. In addition, to estimate the heat transfer in path 2, changes in the temperature of the vibrating beam are measured as shown in Fig. 7. When the heat source is heated to 98 °C, the temperature of the lower beam is increased to 36 °C as a result of heat transfer through air. When induced, acoustic streaming causes the temperature of the vibrating beam to drop to 26 °C in 2 min, which is 6 °C higher than the room temperature. It is also observed that the resulting temperature drop changes with the gap.

III. THEORY

Nyborg (1958) formulated the equation for near-boundary acoustic streaming using successive approximation method as

$$\mu\nabla^2 u_2 - \nabla P_2 + F = 0, \tag{1}$$

$$F \equiv -\rho_0 \langle (u_1 \cdot \nabla) u_1 + u_1 (\nabla \cdot u_1) \rangle, \tag{2}$$

where μ is kinematic viscosity, ρ_0 is constant equilibrium density, u_1 is oscillatory particle velocity, u_2 is acoustic streaming velocity, P_2 is a steady-state "dc" pressure, F is

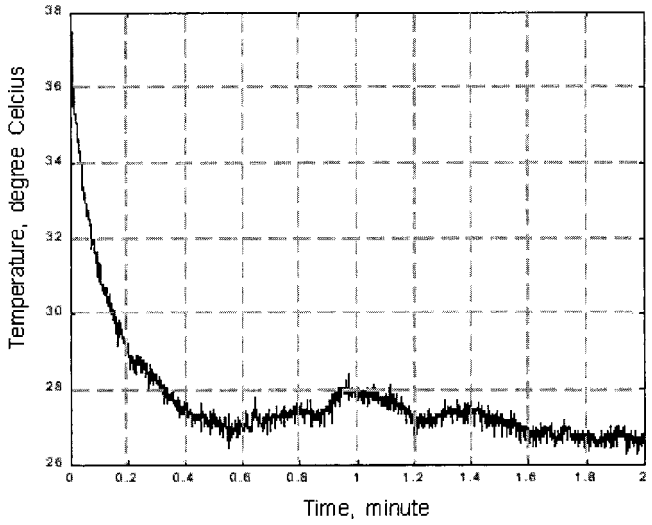

FIG. 7. Temperature drop of the vibrating beam.

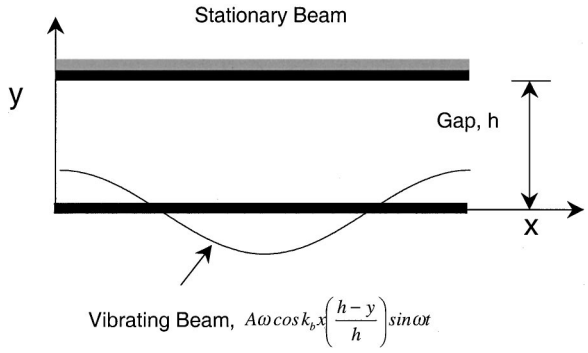

FIG. 8. Simulation schematic drawing.

nonlinear driving forcing term, and $\langle\ \rangle$ means a time average over a large number of cycles. Without averaging, F contains a dc part and harmonically varying terms. The former induces acoustic streaming. When averaged over a relatively long period of time, the effect of harmonically varying forcing terms disappears and only the contributions from the dc part appear in the solution. The acoustic streaming velocity, u_2, approaches a constant value as the distance from the vibrating beam approaches infinity. This time-independent limiting velocity, U_L, is given by

$$U_L = -\frac{3}{4\omega} U_0 \left(\frac{dU_0}{dx}\right), \tag{3}$$

where ω is excitation frequency and U_0 is amplitude of the irrotational velocity tangent to the boundary (cf. Andres and Ingard, 1953). To calculate outer acoustic streaming motion, the limiting velocity, U_L, is used as a slip velocity at the solid surface by assuming Stoke boundary layer thickness negligible (cf. Lighthill, 1978).

The amplitude of the tangential irrotational velocity, U_0, is obtained from the normal irrotational velocity, V, imposing the zero-divergence condition assumed in the Nyborg's formulation. For a relatively small gap, the normal irrotational velocity is assumed to be

$$V = A\omega \cos k_b x \left(\frac{h-y}{h}\right) \sin \omega t = V_0 \sin \omega t, \tag{4}$$

where A is the peak vibration amplitude of an elastic beam, k_b is the bending wave number of the beam defined as $2\pi/\lambda_b$ where λ_b is the wavelength of the beam, and h is the gap between the vibrating beam and the stationary beam as shown in Fig. 8. Equation (4) satisfies the boundary conditions that V at $y=0$ is equal to the velocity of the vibrating beam and V at $y=h$ is zero. By making use of the zero-divergence condition, $\partial U_0/\partial x + \partial V_0/\partial y = 0$, the amplitude of the tangential velocity, U_0, is given by

$$U_0 = \frac{A\omega}{2\pi} \left(\frac{\lambda_b}{h}\right) \sin k_b x. \tag{5}$$

Upon substitution of Eq. (5) into Eq. (3), U_L can be rewritten as

$$U_L = -\frac{3}{8} f \lambda_b \left(\frac{A}{h}\right)^2 \sin 2k_b x, \tag{6}$$

where f is excitation frequency in Hertz.

First, note that, from Eq. (6), any explicit dependence of acoustic streaming velocity on μ disappears although it originates from the viscosity. Also, note that acoustic streaming velocity is a function of the wavelength of the beam and the gap in addition to the excitation frequency and the vibration amplitude.

IV. COMPUTATIONAL FLUID DYNAMICS (CFD) SIMULATION

The length of the two plates for the computational simulations is the same as the wavelength of the ultrasonic flexural standing wave (UFSW). The gap between the two plates is small, i.e., 2–20 mm, and the maximum speed of the air is less than 2 m/s. Thus, the Reynolds number based on the given conditions is less than 1800, which is in the range of laminar flow. The air speed in the gap is under Mach 0.3, so that the incompressible fluid flow assumption may be applicable for a first-order approximation. The governing equations (cf. Kleinstreuer, 1997) for incompressible transient laminar Newtonian fluid flow are continuity,

$$\nabla \cdot \vec{\mathbf{v}} = 0, \tag{7}$$

and linear momentum

$$\frac{\partial \vec{\mathbf{v}}}{\partial t} + (\vec{\mathbf{v}} \cdot \nabla)\vec{\mathbf{v}} = \frac{1}{\rho}(-\nabla p + \mu \nabla^2 \vec{\mathbf{v}}). \tag{8}$$

The boundary condition for the lower vibrating plate of the CFD simulation is the vertical displacement defined by

$$y_p(x,t) = A(t) \cdot \cos(2\pi x/\lambda)$$

$$\text{where } A(t) = A_0 \cdot \sin(\omega t). \tag{9}$$

Here $A(t)$ is the vibration amplitude, λ is the wavelength, A_0 is the maximum vibration amplitude, $\omega = 2\pi f$ is the angular velocity of the wave, f is the frequency, and t is the time. The two open sides constitute natural symmetry planes with zero-gradient conditions.

The simulation covers more than 4000 periods with 16 time steps each to get the quasi-steady state solution. The velocity $\vec{\mathbf{v}}$, which contains harmonic terms and a ''dc'' term, is calculated from Eqs. (7) and (8). The acoustic streaming velocity ($\overline{v}_{a,i}$, $i = x$, y, and z) is obtained by averaging $\vec{\mathbf{v}}$ over a period as follows:

$$\overline{v}_{a,i} = \frac{1}{T_a}\int_0^{T_a} v_i \, dt, \quad i = x, y, \text{ and } z, \tag{10}$$

where T_a is the period of ultrasonic vibration.

A. Numerical analysis

The computational fluid dynamics package CFX 4 (AEA Technology, Bethel Park, PA) was used for the numerical simulation. CFX 4 is a control-volume-based solver and employs a structured, multi-block, body-fitted coordinate discretization scheme, which uses the SIMPLEC algorithm for the pressure correction. The CFD simulation was run on a SGI Origin 2000 (400 MHz; multiple R12000 processors) at the North Carolina Supercomputing Center (NCSC, RTP). Simulations consisted of first determining the instantaneous velocity field, governed by Eqs. (7) and (8) with the moving boundary condition defined by Eq. (1). The time-averaged velocity, i.e., acoustic streaming velocity, was calculated with Eq. (10). CFX 4.3 employs a particular implementation of an Algebraic Multi-Grid called Additive Correction. This approach takes advantage of the fact that the discrete equations are representative of the balance of conserved quantities over a finite volume, making it ideally suited for the discretization used. Coarser mesh equations can be generated by merging the original finite volumes into larger ones. Thus, they impose conservation requirements over larger volumes and in so doing reduce the error components at longer wavelengths. The size and configuration of the computational domain used in this study were adjusted until an acceptable level of grid independence of the final solution was achieved, i.e., $\varepsilon \leqslant 10^{-4}$, where ε represents the mass and momentum residuals.

The algebraic equations are discretized with respect to the computational space coordinates with implementation of the appropriate boundary conditions, i.e., no-slip at the walls and zero-gradients at the symmetry planes. A time-dependent moving grid option was employed, based on a user-supplied FORTRAN program, to solve for the airflow field induced by ultrasonic flexible waves (UFW) at the vibrating plate boundary. This program allows specifying time-dependent grid positions on the lower wall surface at each time step as defined in Eq. (1). The typical size of the computational mesh at about 2000 control volumes and about 3.0 CPU hours on the SGI Origin 2000 were required to obtain the quasi-equilibrium flow field solution. The time-dependent waveform for the UFW was discretized nonlinearly into about 16 time steps for each period. The numerical accuracy of the model is further documented with validation results discussed in the next section.

B. CFD results

Figure 9 shows the time evolution of vortices in the gap between two infinite beams due to acoustic streaming. At time $t = 0$, no airflow exists in the gap, and then the lower beam starts to vibrate with the frequency $f = 28.4$ kHz, vibration amplitude $A = 20\,\mu$m, and wavelength of $\lambda_b = 2.0$ cm in a 2-mm gap between two beams. Four vortices over a single wavelength emerge near the lower vibrating beam [cf. Fig. 9(a)]. They appear between nodal points and antinodal points of the vibrating beam with the two in the center moving closer to each other [cf. Figs. 9(a)–(l)]. The airflow patterns show an upward motion at antinodal points and downward at nodal points, which is similar to the experimental visualization shown in Fig. 2. After 610 pulses, a steady streaming flow field is achieved [cf. Figs. 9(f)–(l)].

Figure 10 represents the acoustic streaming velocity tangent and normal to the beam along a fictitious vertical line passing through a vortex center. The tangential and normal velocities are zero at the vortex center (about $y = 0.072$ cm). The tangential velocity reaches 70 cm/s near the lower vibrating beam and 30 cm/s near the upper beam. The normal velocity is significant only near the nodal and antinodal points, and near zero along the vertical line through the vortex center as shown in the flow field of the converged solution in Fig. 9(l).

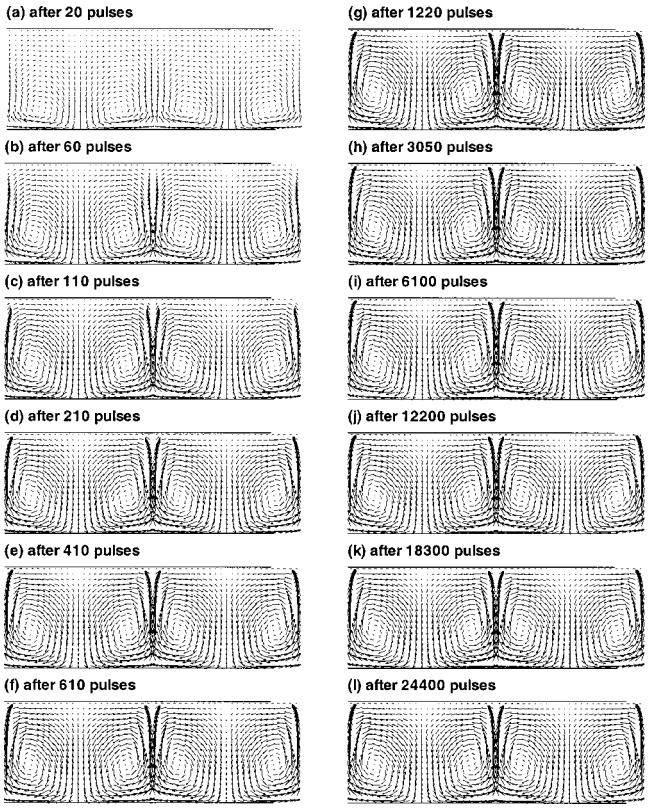

FIG. 9. Time evolution of the streaming velocity field for the base case.

To observe the effect of changing excitation frequency, vibration amplitude, and gap on the streaming velocity and its patterns, a series of simulations was conducted. It is observed that the vortical flow patterns are not influenced by the simulation conditions but the magnitude of the acoustic streaming velocity is strongly influenced. Therefore, for the following analyses, only the variations of the streaming velocity magnitude along a vortex center are compared and discussed, except for the case of open ends in Sec. IV B 3.

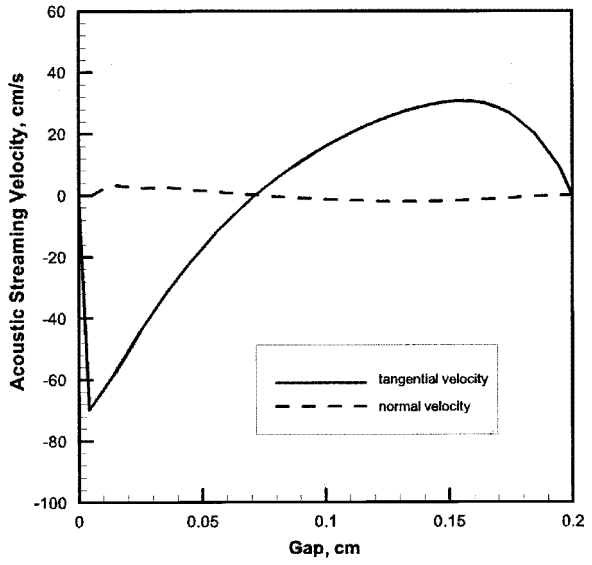

FIG. 10. The streaming velocity through the vortex center.

TABLE I. System characteristics for CFD simulation.

Frequency (kHz)	Vibration amplitude (μm)	Velocity of vibrating beam (m/s)	Wavelength (mm)
6.0	93.0	3.5	48.0
12.0	47.0	3.5	34.0
18.0	31.0	3.5	28.0
28.4	20.0	3.5	20.0
50.0	11.0	3.5	17.0

1. Effect of vibration frequency

The effect of the excitation frequency on the acoustic streaming velocity is measured. Of particular interest is to observe a change in acoustic streaming velocity when the excitation frequency becomes ultrasonic. If the excitation frequency of the beam increases, the irrotational velocity would also increase with the excitation frequency. This results in an increase in acoustic streaming velocity because acoustic streaming velocity is proportional to the square of the irrotational velocity (cf. Nyborg, 1958). Therefore, the effect of excitation frequency can be properly measured only when the velocity of the vibrating beam is maintained at a constant value. This can be achieved by decreasing the vibration amplitude to an appropriate value. Detailed test conditions are shown in Table I.

Figure 11 shows the maximum acoustic streaming velocity in the 2-mm gap at an excitation frequency of 6, 12, 18, 28.4, and 50 kHz with corresponding vibration amplitude values detailed in Table I. The results are obtained from CFD simulation and the analytical solution based on Eq. (6). It is observed that the maximum streaming velocities decrease with the excitation frequency. The maximum streaming velocities at 28.4 kHz near the lower and upper beams are 66.2 and 30.6 cm/s, respectively. While the streaming patterns around the lower beam are directly influenced by the beam motion, those near the upper beam are induced by the streaming flows from the lower beam. It is observed that the airflow is attenuated in the process of inducing streaming motions near the upper beam. As a result, the larger streaming velocities are observed near the lower beam. As shown in

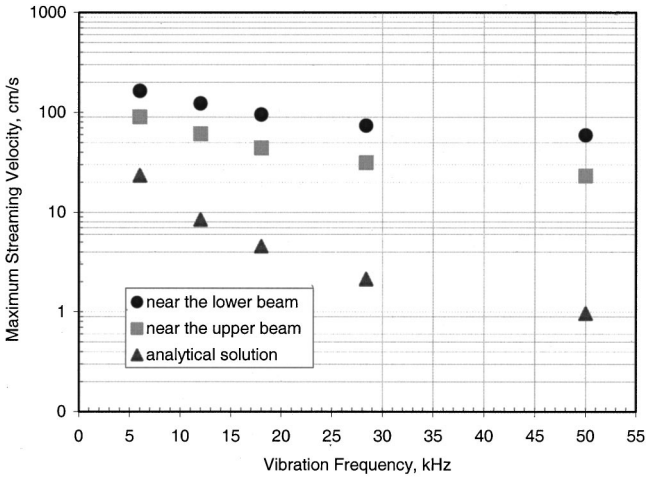

FIG. 11. The maximum acoustic streaming velocity for constant vibration velocity of the beam.

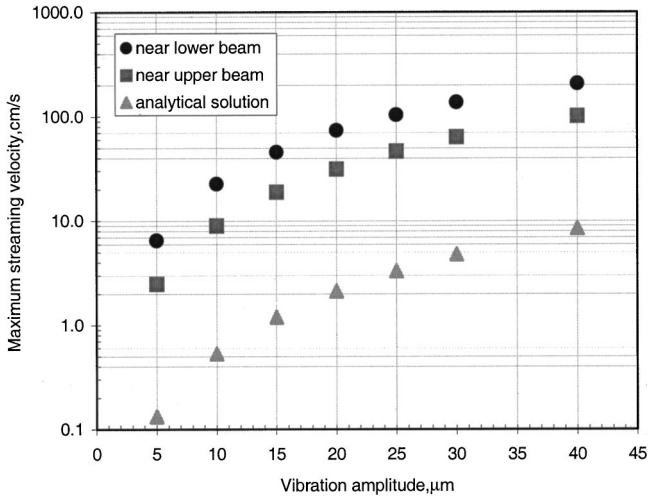

FIG. 12. The maximum acoustic streaming velocity for different vibration amplitude.

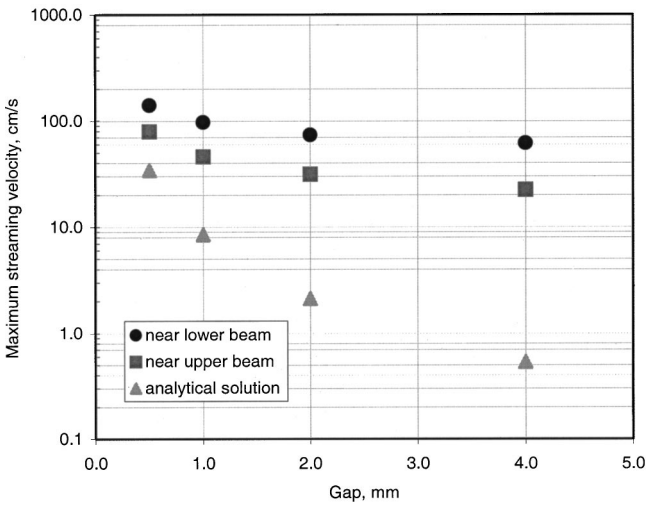

FIG. 13. The maximum acoustic streaming velocity for different gap size.

Eq. (6), the acoustic streaming velocity is proportional to the square of the vibration amplitude and the wavelength of the vibrating beam that decreases with the excitation frequency. Although the excitation frequency grows, a decrease in wavelength and vibration amplitude offsets the increase in the acoustic streaming velocity due to frequency increase. As a result, both CFD simulation and the analytical solution indicate that the maximum streaming velocity decreases with excitation frequency.

Moreover, no significant change in acoustic streaming velocity is observed as the excitation frequency becomes ultrasonic. The analytical solution does not include the attenuation of flow, resulting in uniform streaming velocities across the gap. Therefore the analytical solution can be compared to the streaming velocity near the lower beam obtained from CFD simulation. It is noted that an analytical solution formulated based on Nyborg's theory underestimates the acoustic streaming velocity when compared to the CFD results, which are based on the assumption of air incompressibility for $\mathrm{Ma} < 0.3$.

2. Effect of vibration amplitude and gap

Figure 12 shows the maximum streaming velocities near the beams for vibration amplitudes of 5, 10, 15, 20, 25, 30, and 40 μm with a gap of 2 mm at an excitation frequency of 28.4 kHz. The wavelength is 20 mm. The maximum streaming velocity increases as the vibration amplitude increases due to increase in the irrotational velocity. The maximum irrotational velocity near the lower vibrating beam can be calculated with the excitation frequency, the vibration amplitude and wavelength of the beam, and the gap.

For vibration amplitude of 25 μm, the maximum streaming velocities near the lower and upper beams from CFD simulation reach 100 and 45 cm/s, respectively. For the same vibration amplitude, a maximum streaming velocity of 3.3 cm/s is obtained from the analytical solution. It is observed that as the vibration amplitude grows, maximum streaming velocity from both CFD simulation and the analytical solution increase in a similar trend, an increase with the square of the amplitude but the analytical solution predicts significantly smaller acoustic streaming velocity. An explanation for this discrepancy requires further investigation.

Figure 13 represents the maximum acoustic streaming velocity as a function of the gap between the vibrating beam and the upper stationary beam. The maximum streaming velocity decreases with the growth of the gap for both CFD simulation and the analytical solution. It is also observed that the analytical solution underestimates acoustic streaming velocity as opposed to CFD simulation result. The difference between the analytical and numerical results grows as the gap increases because the analytical model is developed with an assumption that the gap is small enough to presume a linear variation of the normal irrotational velocity across the gap.

3. Effect of beam end openings

Figure 14 shows the streaming velocity fields for the 2 mm gap, considering the lower beam to be one-and-a-half-wavelength long (3 cm) and the upper beam one-wavelength long (2 cm) to observe the effect of an open-ended channel. Vortical flow and flow entrainment are observed near the

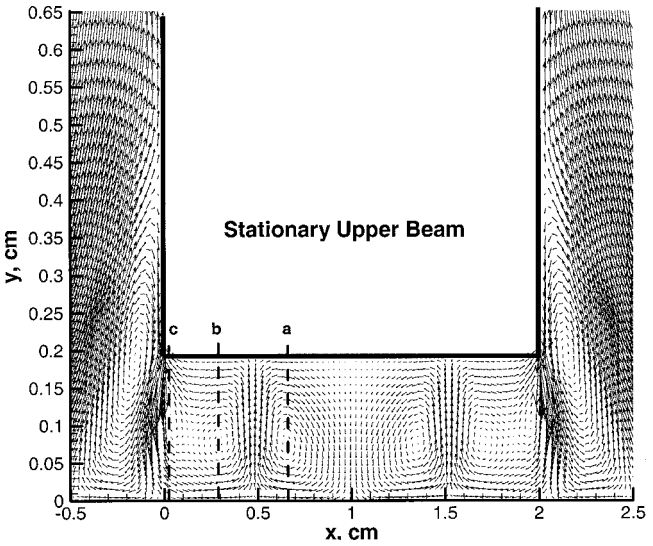

FIG. 14. The streaming velocity considering the entire system.

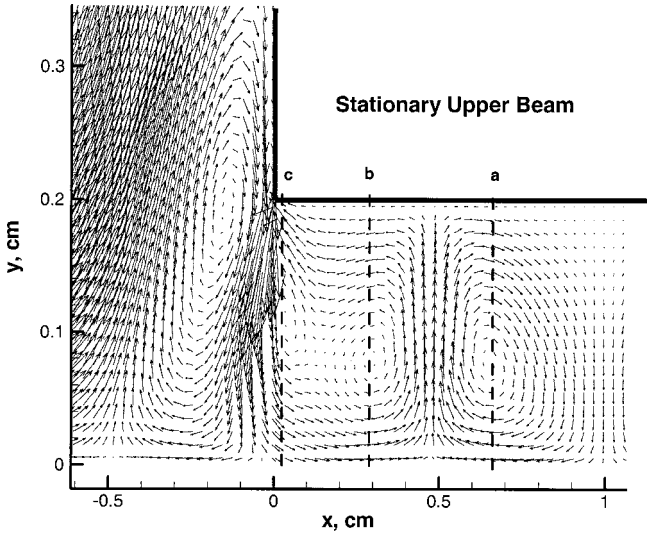

FIG. 15. Enlarged view of the streaming velocity fields near the end.

ends of the upper beam. The vortex centers in the channel are located at $x=0.3$ and 0.65 cm with a symmetry condition at $x=1$ cm. Due to air entrainment, the flow field near the end is disturbed, forming a small vortex (cf. enlarged Fig. 15). Figure 16 shows the magnitude of the acoustic streaming velocity in the gap from a three-dimensional perspective. A maximum streaming velocity occurs right at the openings of the gap near the upper beam, which enhances the mixing of flow between inside and outside the gap. The streaming velocities near the lower beam are generally greater than those near the upper beam except the maximum streaming velocity occurring at the openings. The velocities observed with an open-ended channel are greater than those without an opening (cf. Fig. 13). The velocity near the lower beam reaches up to 130 cm/s due to the flow entrainment and is almost twice that of the 2-mm gap case without flow entrainment. From this, one concludes that flow entrainment enhances the flow speed and changes the flow pattern, resulting in enhanced cooling capability.

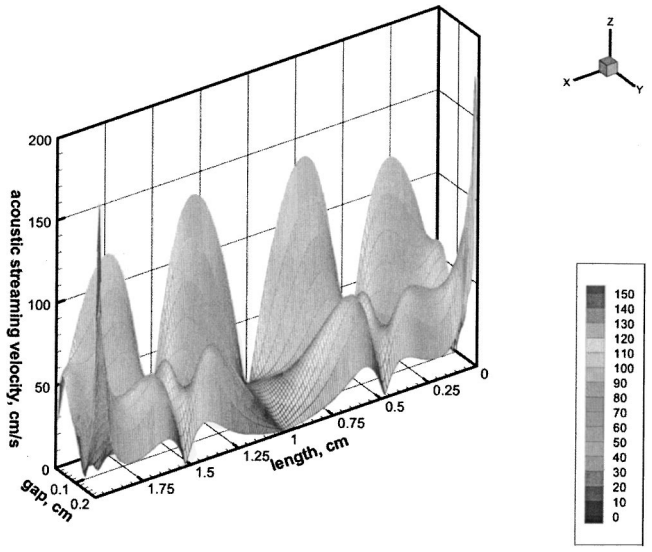

FIG. 16. The 3-D streaming velocity contours inside the gap between two plates.

V. CONCLUSIONS

An investigation of acoustic streaming induced by the ultrasonic flexural vibration is presented. The investigation includes acoustic streaming pattern and its velocity along with associated heat transfer characteristics. Acoustic streaming patterns visualized using acetone corresponded well with the prediction by Nyborg's theory. Using acoustic streaming, a notable temperature drop of 40 °C was obtained in 4 min and maintained. Tests identifying major heat flow paths indicated that both gaps and the vibrating beam serve as crucial heat flow paths.

Employing CFD simulations assuming laminar incompressible flow, it was shown that the vortical flows, observed by experiment and predicted by acoustic streaming theory, could be reproduced. Also, it was found that the streaming velocity from the CFD simulation is far greater than the estimation from the analytical solution based on sonically induced acoustic streaming assuming inviscid flow and a linear variation of the normal (irrotational) velocity across a very small gap (cf. Nyborg, 1958; Vainshtein *et al.*, 1995). This result proves that the theoretical calculations based on sonically induced acoustic streaming may not be extended to estimate ultrasonically induced acoustic streaming velocities. In other words, more comprehensive CFD simulations considering turbulent and/or compressible flow may be needed to accurately predict ultrasonically induced acoustic streaming flows.

With an open-ended channel, simulation revealed the existence of large flow entrainment at the channel ends, which enhances convective heat transfer but cannot be captured with the analytical solution due to the complexity of boundary conditions. With a computational control volume mesh of 2000, the CFD simulation of the flow field induced by a beam vibrating at an ultrasonic frequency is computationally very intensive. It takes almost 10 CPU hours on the Cray T-90 supercomputer and 90 CPU hours on SGI Origin 2000 to obtain a fully developed acoustic streaming flow field. Although the CFD simulations are expensive, more accurate and realistic results can be obtained including a three-dimensional effect of acoustic streaming and the open-ended channel.

Andres, J. M., and Ingard, U. (**1953**). ''Acoustic streaming at high Reynolds numbers,'' J. Acoust. Soc. Am. **25**(5), 928–937.

Chen, Z. D., Taylor, M. P., and Chen, J. J. J. (**1998**). *Heat Transfer on a Surface Affected by an Air/Water Interface Undergoing Wave Motion* (The Minerals, Metals & Materials Society), pp. 429–435.

Fand, R. M., and Kave, J. (**1960**). ''Acoustic streaming near a heated cylinder,'' J. Acoust. Soc. Am. **32**(5), 579–584.

Faraday, M. (**1831**). Philos. Trans. **121**, 229.

Gopinath, A., and Mills, F. (**1993**). ''Convective Heat Transfer From a Sphere Due to Acoustic Streaming,'' J. Heat Transfer **115**, 332–341.

Gopinath, A., and Mills, F. (**1994**). ''Convective Heat Transfer Due to Acoustic Streaming across the Ends of Kundt Tube,'' J. Heat Transfer **116**, 47–53.

Gould, R. K. (**1966**). ''Heat transfer across a solid-liquid interface in the presence of acoustic streaming,'' J. Acoust. Soc. Am. **40**(1), 219–225.

Hamilton, M. F., and Blockstock, D. T. (**1998**). *Nonlinear Acoustics* (Academic, New York).

Ingard, U., and Labate, S. (**1950**). ''Acoustic circulation effects and the nonlinear impedance of orifices,'' J. Acoust. Soc. Am. **22**(2), 211–218.

Jackson, F. J., and Nyborg, W. L. (**1960**). ''Sonically induced microstreaming near a plane boundary. I. The sonic generator and associated acoustic fields,'' J. Acoust. Soc. Am. **32**(10), 1243–1250.
Kays, W. M., and Crawford, M. E. (**1993**). *Convective Heat and Mass Transfer* (McGraw–Hill, New York).
Kleinstreuer, C. (**1997**). *Engineering Fluid Dynamics–An Interdisciplinary Systems Approach* (Cambridge U.P., New York).
Lee, C. P., and Wang, T. G. (**1990**). ''Outer acoustic streaming,'' J. Acoust. Soc. Am. **88**(5), 2367–2375.
Lighthill, J. (**1978**). ''Acoustic Streaming,'' J. Sound Vib. **61**(3), 391–418.
Nguyen, N. T., and White, R. M. (**1999**). ''Design and Optimization of an Ultrasonic Flexural Wave Micropump using Numerical Simulation,'' Sensors Actuators **77**, 229–236.
Nyborg, W. L. (**1958**). ''Acoustic Streaming near a Boundary,'' J. Acoust. Soc. Am. **30**(4), 329–339.
Rayleigh, Lord (**1945**). *Theory of Sound* (Dover, New York).
Ro, P. I., and Loh, B. (**2001**). ''Feasibility of using Ultrasonic Flexural Waves as a Cooling Mechanism,'' *IEEE Industrial Electronics* Vol. 48, No. 1, pp. 143–150.
Sashida, T. (**1993**). *An Introduction to Ultrasonic Motors* (Clarendon, Oxford).
Schlicting, H. (**1955**). *Boundary Layer Theory* (McGraw–Hill, New York).
Uhlenwinkel, V., Meng, R., Bauckhage, K., Schreckenber, P., and Andersen, O. (**1994**). ''Heat Transfer to Cylindrical Bodies and Small Particles in an Ultrasonic Standing-Wave Fields of Melt Atomizer,'' in *Multiphase-Flow and Heat Transfer in Materials Processing*, ASME, FED-Vol. 201/HTD-Vol. 297, pp. 19–24.
Vainshtein, P., Fichman, M., and Cutfinger, C. (**1995**). ''Acoustic enhancement of heat transfer between two parallel plates,'' Int. J. Heat Mass Transf. **38**(**10**), 1893–1899.